6

W/SS thin film as a high-temperature infrared reflector for solar thermal applications: Intrinsic properties and impact of residual oxygen

6.1 Introduction

Solar thermal technology is being explored for a variety of applications ranging from power generation to heating and cooling applications. In such applications, higher thermal efficiency may increase the overall solar thermal performances. It can be achieved with efficient absorption of incoming solar radiation and its conversion into thermal energy with minimum heat losses. Specially designed selective surface with high absorptance in UV-Vis-NIR range (0.3 – 2.5 μm) and low-emittance in IR range (2.5 – 25 μm) can fulfill this requirement [Kennedy, 2002, Zhang & Mills, 1992]. So far, various spectrally selective structures were proposed for this purpose. The cermet based coating consisting of single or multiple layers is the most common among various SSACs. These structures show better optical properties compared to other selective surfaces [Zhang & Shen, 2004, Zhang, 2000, Esposito et al., 2009]. Most of such SSACs are used up to mid-temperature range, whereas very few are suitable for high-temperature applications. In cermet composites, metal components are prone to oxidation at elevated temperature, and thus, degrading the optical characteristic of the selective surfaces. Also, to minimize the thermal losses and avoid interdiffusion, the metallic layer as an IR reflector is usually introduced beneath the selective solar absorber surfaces. These metallic IR layers are also prone to the oxidation, and at higher temperature probability of interdiffusion is also more from the IR layer to the cermet layer or from substrate to IR layer or both. This can be mitigated by a stable high temperature stable infrared layer in these selective surfaces. The commonly used metals for IR reflector in SSACs are nickel , tungsten, aluminum, molybdenum, silver (Ag) and zirconium [Bogaerts & Lampert, 1983, Pettit & powell, 1980, Sathiaraj et al., 1990, Martin et al., 1982, Donnadieu & Seraphin, 1978, Usmani & Dixit, 2016, Sibin et al., 2015]. These IR reflector layers are deposited using different coating routes such as sputtering, electrodeposition, and evaporation. Among them, sputtering is the most commonly used for depositing IR layer. Metal are chosen for the IR reflector layer on the basis of the operating temperature range. For mid-temperature (< 350 °C) spectrally selective solar absorber gold, nickel, silver and aluminum are used whereas for high temperature (> 400°C) spectrally selective solar absorber, high melting point metals such as platinum, molybdenum and zirconium are utilized for IR reflector layer due to their high thermal stability. It has been reported that Nickel can be used as an IR layer up to 400°C with better thermal stability (Muehlratzer et al., 1981]. However, at higher temperatures, these metals may diffuse into the absorber structure, degrading the optical performance of selective surface [Lee et al., 2000]. Silver can be used for the IR layer for operating temperature < 350°C as at 350°C due to agglomeration, the IR reflecting properties are affected, so over all-optical and thermal performance of the selective absorber surfaces degrades. Al as IR reflector layer shows similar behavior [Ihara et al.,1977]. SSAC with Zirconium as an IR layer is used because of its refractory nature in SSACs [Lazarov and Mayer, 1998, Usmani & Dixit, 2016]. Further, chromium, gold, platinum, and molybdenum are also investigated as the IR layer [Morales & Ajona, 1999, Fan & Zavracky, 1976, Thornton & Lamb, 1981]. But the higher cost of these metals is prohibiting their use as the IR layer for practical applications. Among the reported selective absorber with an IR

layer are mostly are stable up to mid-temperature range. At higher temperatures, these structures are stable in vacuum only [Usmani & Dixit, 2016]. The high-temperature durable metal such as tungsten and molybdenum also explored and reported for IR layer application. Tungsten has high melting point (~3422°C) and also shows poor oxidation tendency in open air conditions. Thus, tungsten offers favorable properties for IR layer in high temperature range. Tungsten thin layers are reported with low thermal emittance ~ 0.03 [Sibin et al., 2015, Zhang et al., 2017). As an aside, there are reports that tungsten will exhibit higher emittance ≥ 0.1 due its intrinsic interband energy transitions causing absorption in wavelength range of 0.4 – 20 μm (Stelmakh et al., 2013, Nomerovaannaya et al., 1971). Also, synthesis technique and presence of residual oxygen during fabrication may lead to the formation of oxide along metallic tungsten, which may also affect the optical properties in UV-Vis-NIR (0.3 – 2.5 μm) as well as in IR (2.5 – 25 μm) range.

The current work is discussing such ambiguities regarding the optical properties of tungsten as the IR reflecting layer. The tungsten thin layer with minimum thermal emittance is deposited using sputtering by optimizing various parameters and characterized intensively. The interband transition and the presence of oxide causing absorption are the limiting factors for observed high thermal emittance, as discussed in the following sections.

6.2 Experimental details

For W deposition cleaned SS substrate used. The cleaning of the SS substrate is explained in section 3.1. W thin film deposited on SS substrate using sputtering in DC power mode. The detailed deposition process explained in section 3.2.3.

6.3 Result and Discussion

The deposition process is optimized by varying the different parameters such as sputtering power, deposition temperature, and duration of deposition to get tungsten thin film on SS substrate with minimum thermal emittance. The sputtering powers used for deposition were 150W, 200W, and 250W. The thin films were deposited at different temperatures, such as room temperature, 200°C, 300°C, and 350°C. Also, films were deposited for one and two hours. **Table 6.1** summarized the deposition parameter used for thin tungsten thin film deposition.

Table 6.1: Deposition condition used for tungsten film on SS substrate using sputtering

DC Power (w)	Deposition temperature (°C)	Duration (minutes)	Thickness (μm)	preheating of Chamber
150	RT	60	0.51	-
150	350	60	0.55	-
150	350	120	0.95	-
150 (Sample A)	450	120	1.00	-
250	RT	60	0.60	-
250	350	60	0.62	-
250	350	120	1.00	-
200	RT	120	1.12	(450°C for 2 hours)

200	200	120	0.98	-do-
200	300	120	0.95	-do-
200 (Sample B)	350	120	1.10	-do-

The thermal emittance of fabricated tungsten thin film on the SS substrate was estimated using equation (2.4) and shown in **Figure 6.1**. The emittance reduces with an increase in deposition power; however, for the film deposited at a lower temperature, deposition power does not play any significant role (**Figure 6.1(a)**). The emittance values of the film deposited for longer duration and at higher temperatures were changing significantly compared to one deposited for a short duration and lower temperatures (Figure 6.1(b)). The impact of temperature on the fabricated film was also studied. Reduction in emittance was observed with increasing the deposition temperature (**Figure 6.1 (a) and (b)**). Also, the emittance decreases with increasing the film thickness up to ~1 μm (Figure 6.1 (c)).

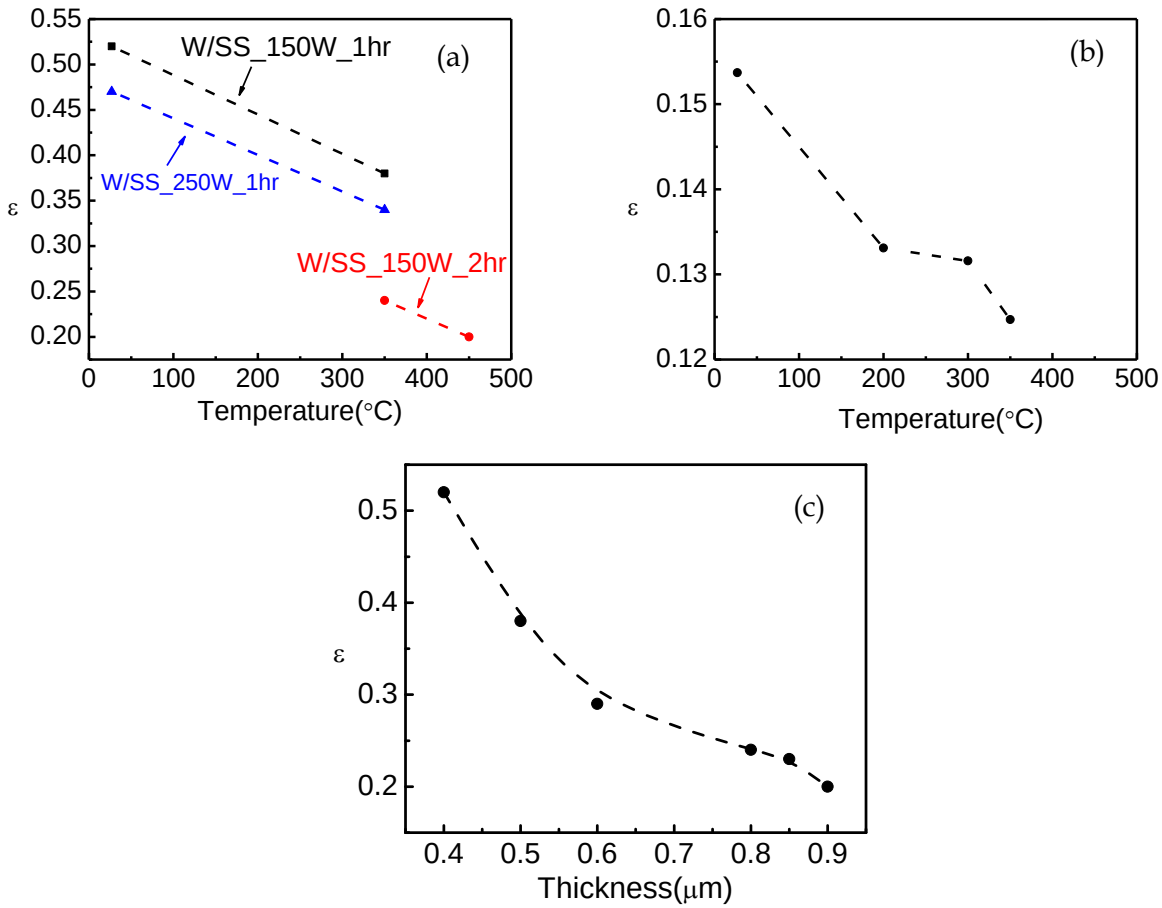

Figure 6.1 Emittance versus temperature of W/SS (Sample A) and (b) W/SS (Sample B) (c) emittance versus thickness

The XRD plot for optimized W thin film with the minimum emittance deposited without preheating and after preheating the chamber shown in **Figure 6.2 (a & b)**. The sample with minimum emittance in case of deposited without preheating called Sample A and sample with minimum emittance deposited in case of after preheating the chamber called sample B. As per XRD spectrum for sample A (**Figure 6.2 (a)**), tungsten peak at 2θ ~ 38°, and 72° matched with

ICDD File No. 04-0806 and 47-1319 [Sibin et al., 2015, Kobayashi et al., 2006] and tungsten oxide peak at 2θ ~34° matched with ICDD File No. 43-1035 [Ozkan et al., 2003]. For sample B, tungsten peak at 2θ ~38° and ~ 57°, 72° matched with ICDD File No. 04-0806 and 47-1319 respectively [12,13]. Also, tungsten oxide peak at 2θ~ 34° matched with ICDD File No. 43-1035) was found [26]. XRD observation suggests the presence of tungsten as well as tungsten oxide in both the sample. Scherrer relation $D=(0.94\times\lambda)/(\beta\times\cos\theta)$ is used to estimate the crystallite size (D), where β is full width at half maxima (FWHM) in radian, λ (λ_{Cu}= 1.5406Å for copper k_{α}) is the characteristic X-ray wavelength of Cu source, and θ is angle of observed peak [Gupta & Dixit, 2017]. Williamsons and Smallman's relation, $\delta=n/D^2$ is used for calculating the dislocation density by putting n=1 (for the minimum dislocation) and value of crystallite size (D) [Williamson & Smallman, 1956]. The strain values for fabricated thin films are estimated using the formula $\varepsilon=\beta\cos\theta/4$. **Table 6.2** summarized the estimated crystallite size, dislocation density and strain values for these samples. Sample B is showing higher crystallite size with respect to sample A and is attributed to the observed lower dislocation density for sample B compared to Sample A. The residual oxygen presence in depositing chamber causes the formation of tungsten oxide in both the sample. The observation of lower intensity of oxide phase in XRD spectrum in case of sample B may be due to the lower residual oxygen presence after preheating the deposition chamber. Lower strain in case of Sample B compared to Sample A also supports the presence of lesser oxide components.

Table 6.2 Crystallographic information of two samples of tungsten layer deposited on the SS substrate

Sample	2θ for (111) W plane (°)	FWHM (°)	Crystallite size(nm)	Dislocation density($\delta \times 10^{16}$) (line m^{-2})	Strain (ε)
Sample A	38.23	1.25	7	2.03	0.295
Sample B	38.22	0.52	16	0.36	0.124

Scanning electron microscopy (SEM) measurements are performed for surface microstructural analysis. **Figure 6.3 (a & b)** shows the captured SEM image fo W/SS thin film. In both images, surface imprint due to grinding and polishing are visible. The elemental composition of tungsten and oxygen present in the sample is analyzed using EDX measurement provided with an SEM instrument. Insets in **Figure 6.3(a & b)** list the elemental composition. The presence of tungsten oxide was observed in both samples, but the presence of oxide content was higher in sample A fabricated without preheating the chamber compared to sample B fabricated after preheating the chamber. These observations suggest that the prepared film is not purely metallic, it consists of W-WO_3 cermet matrix. The estimated metallic tungsten volume fraction as per EDX measurement was ~ 0.67, and WO_3 volume fraction was ~ 0.33 for Sample A, however, for sample B, higher tungsten metallic fraction up to ~ 0.72 and reduced WO_3 content was observed. Surface topographical measurement for the prepared W/SS thin film was performed using AFM measurement to study surface roughness and its impact on optical properties of prepared W/SS film. The surface scanning was carried out in contact mode of operation. 5 x 5 μm^2 area was scanned, and the captured topographical image has resolution of 256 x 256 pixels. **Figures 6.4(a & b)** show the three-dimensional topographical image of deposited W/SS fabricated sample A and sample B. The measured RMS surface roughness of Sample A and Sample B was ~66.36 ± 3 nm and 19.47 ± 1.5 nm respectively. These observations suggest that the lower surface roughness and smaller oxide content presence attributing to lower thermal emittance for sample B. Further, the surface morphology analysis suggests the granular growth and larger grain in case of sample B as compared to sample A. Similar results were observed in XRD measurement as mention in **Table 6.2**.

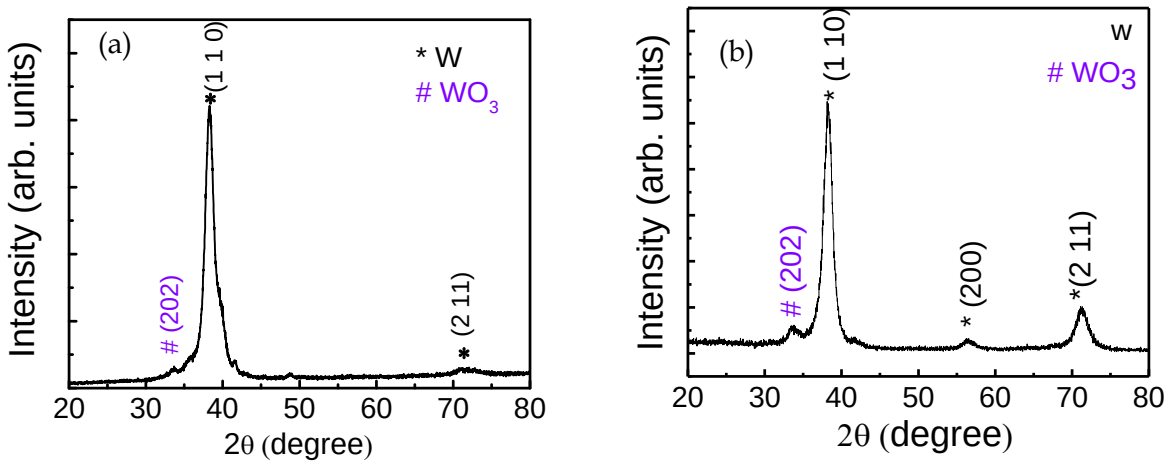

Figure 6.2 XRD plot of W/SS fabricated thin film (a) Sample A and (b) Sample B

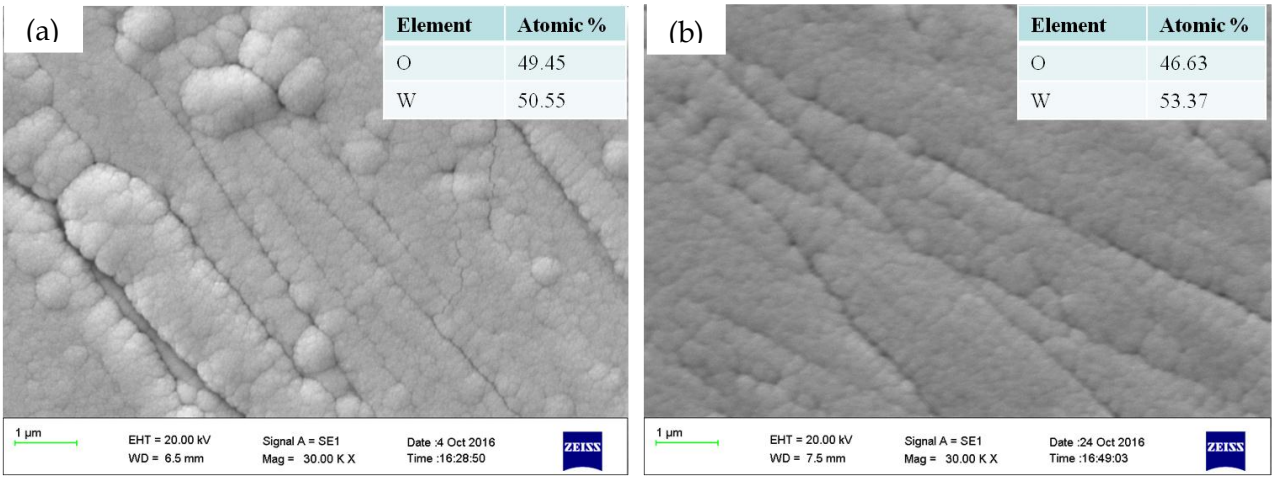

Figure 6.3 (a) SEM images of W/SS fabricated thin film (a) Sample A and (b) Sample B

(a) W/SS (Sample A) and (b) W/SS with (sample B)

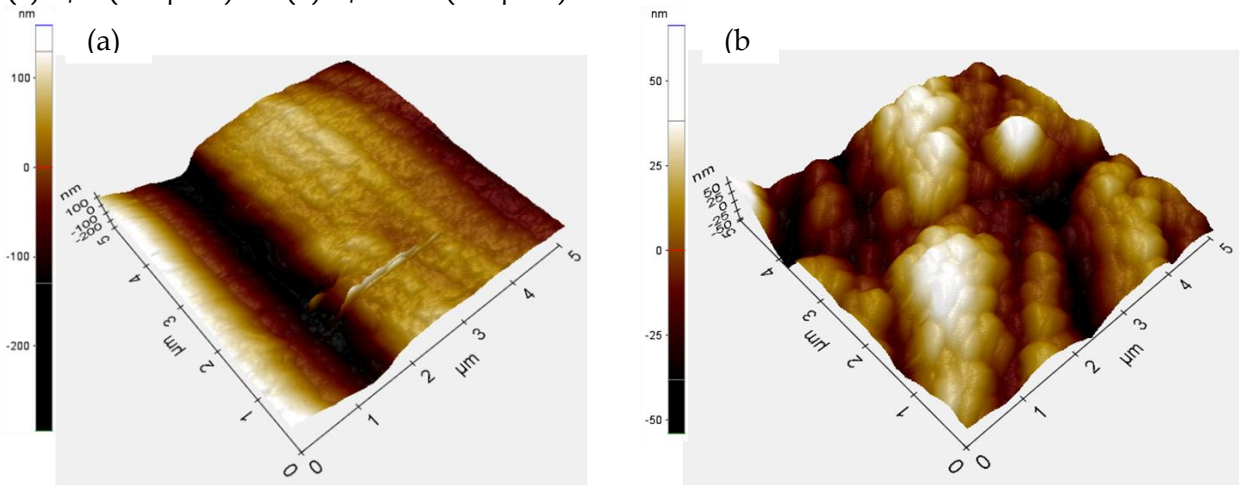

Figure 6.4 3-D topographic image of W/SS fabricated thin film (a) Sample A and (b) Sample B

6.4 Optical characterization

The reflectance measurement of the fabricated W/SS thin film was performed using FTIR spectrophotometry. **Figure 6.5(a & b)** represents the measured reflectance versus wavelength plot of W/SS thin film for sample A and sample B, respectively. The emittance was estimated using reflectance data and equation (2.4). The observed emittance for both the sample is higher, and even for sample B, it is ~ 0.13. It is due to the interband transition in tungsten. The theoretical and experimental evidence shows the splitting of d orbital due to spin-orbital interaction [Nomerovaannaya et al., 1971, Mattheiss & Watson, 1964, Loucks, 1965]. These splitted band lies at 0.33 & 0.4 eV near Fermi level. Additionally, there are two low energy gaps between 3 - 4 and 4 – 5 electronic states exist (Nomerovaannaya et al., 1971). The energy gaps for these states were estimated by Mattheiss and Watson [Mattheiss & Watson, 1964] and Loucks [Loucks, 1965] and found to be ~ 0.4-0.5 eV.

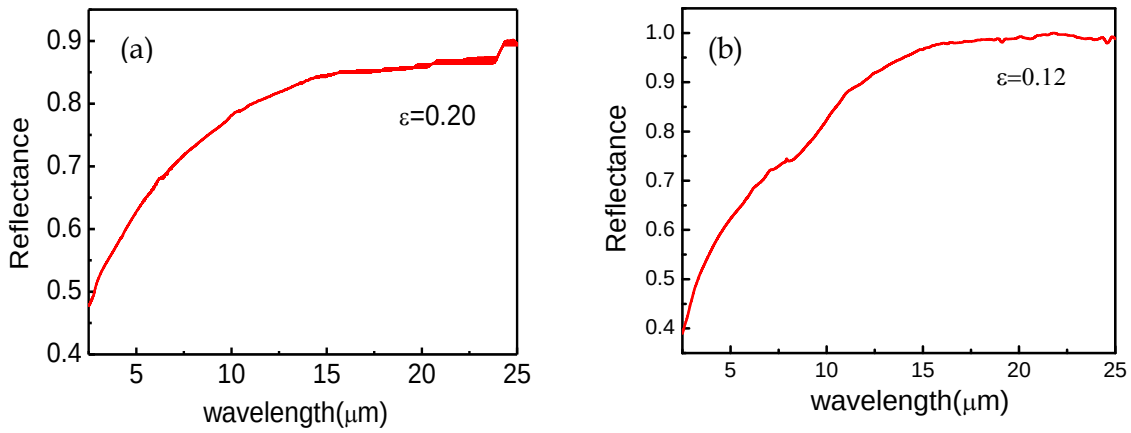

Figure 6.5 Reflectance plot with wavelength of W/SS fabricated thin film (a) Sample A and (b) Sample B

Figure 6.6 presents the reflectance and absorption together with the energy band diagram. It also shows the tungsten 5d orbital splitting due to spin-orbit interaction and Interband transitions. The bandgap of tungsten oxide (WO_3) ~ 2.6-2.8 eV is also shown schematically. The presence of interband energy gap ~ 0.4 and 0.5 eV in tungsten is responsible for IR range absorption, which ultimately increases emittance. Also, the interband transition around 0.3 eV causes the absorption in the low wavelength range below 4 μm [Nomerovaannaya et al., 1971, Bermel et al, 2012]. It was also observed that the sample A with high oxide content shows high emittance~ 0.2 compared to emittance ~ 0.12 of sample B with low oxide content. These observations suggest that the interband transition in 4-20 μm range, plasmonic absorption ` 1.75 eV, and tungsten oxide presence collectively responsible for low reflectance or higher emittance of fabricated W/SS thin film. The absorption in visible range is also possible as tungsten oxide has bandgap in 2.6- 2.8 eV range. We further performed diffuse reflectance measurement and estimated the absorption to study the impact of oxide on the reflectance of the developed W/SS thin layer as shown in **Figure 6.6(a)**. The observed absorptance in the visible range was strong. Bandgap absorption due to the presence of WO_3, plasmonic absorption over the visible range (~ 1.75 eV), and absorption influenced by metal-dielectric composite presence in W/SS thin film is collectively causing this absorption.

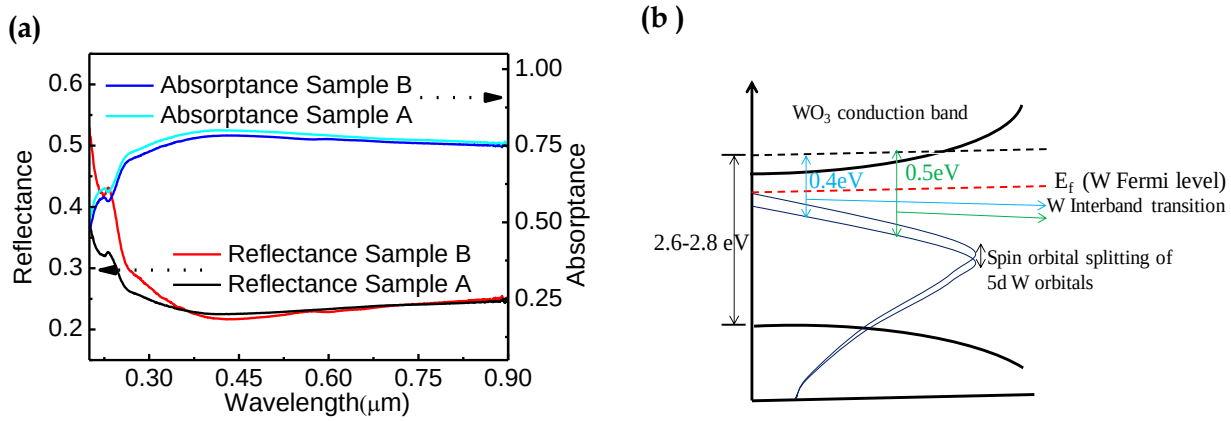

Figure 6.6 (a) The schematic of UV-Vis absorption for W/SS Sample A and Sample B thin films and (b) an schematic diagram, showing tungsten oxide band gap and tungsten intraband energy levels with spin-orbit coupling

Also reflectance data used to calculate the refractive index and extinction coefficient using equation

$$n = \frac{(1+R)^2}{(1-R)^2} \tag{6.1}$$

$$k = \alpha\lambda/4\pi \tag{6.2}$$

Where n and k are refractive and extinction coefficient, respectively.; α denotes the absorption coefficient [Griffiths, 1999]. Absorption coefficient α is estimated using Kubelka–Munk relation $\alpha = (1-R)^2/2R$ where R means reflectance [Kubelka & Munk, 1931]. **Figure 6.7(a & b)** shows the refractive index and extinction coefficient plots with wavelength, respectively for the fabricated W/SS thin film sample A and sample B. Here, both n and k are increasing with wavelength, confirming the metallic nature as reported in literature [Selvakumar et al., 2010b, Xinkang et al., 2008].

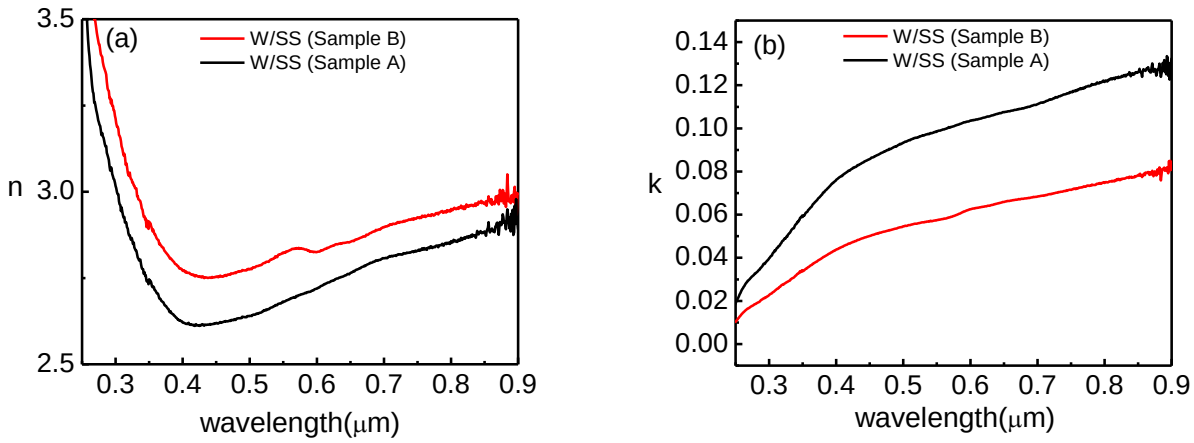

Figure 6.7 (a) Refractive index 'n' with wavelength and (b) extinction coefficient 'k' versus wavelength plot of W/SS sample A and sample B

The fabricated W/SS thin film sample with lower oxide presence shows a higher extinction coefficient compared the sample B containing lower oxide content. The higher oxide presence is also causing the absorptance along with plasmonic absorption and intrinsic

interband transition. The estimated absorptance was 78% and 76 % for sample A and sample B, respectively, substantiating the observed higher emittance for fabricated W/SS thin film. Thus, the residual oxygen causing the oxide formation, which in turn hamper the optical properties of deposited W/SS thin film in the IR range. So for development of W/SS thin film as IR reflector layer with lower thermal emittance, the deposition must be performed in oxygen free environment. However, the intrinsic interband transition in tungsten limits the development of W/SS thin film with thermal emittance ~ 0.1 or less than 0.1.

6.5 Conclusion

The W/SS thin film fabricated using sputtering with thickness in micrometer range at higher temperatures showed lower emittance. The lowest thermal emittance ~ 0.13 is observed for W/SS thin film fabricated after preheating the chamber. The intrinsic W interband transition and plasmonic absorption around 1.75 eV in visible range and formation of oxide collectively limit the emittance of W/SS thin film near ~ 0.1.